1 # Fe-Ni ideality during core formation on Earth

2 **DONGYANG HUANG[1], JAMES BADRO[1,2]**

3 [1]Institut de Physique du Globe de Paris, Sorbonne Paris Cité, 75005 Paris, France

4 [2]École Polytechnique Fédérale de Lausanne, CH-1015 Lausanne, Switzerland

5 **ABSTRACT**

6 Earth's core is essentially composed of a light-element bearing iron-nickel alloy (Birch 1964).

7 The nickel content in the core has negligible effects on physical properties such as density and

8 compressibility (e.g., Lin et al., 2003; Kantor et al., 2007; Martorell et al., 2013; Badro et al.

9 2014). This deters any attempt to determine or even estimate the nickel content of the core using

10 seismological models, as in the case of light elements. It was recently proposed that the presence

11 of nickel should fractionate iron isotopes in small planetary cores (Elardo and Shahar 2017), but

12 the effect for a large (hot) planet such as the Earth would not be measurable; this observation

13 however opens up the possibility that Ni can have an effect on element partitioning between the

14 metallic alloy and the silicate melt during core formation. In this case, the siderophile trace-

15 element composition of the mantle would in turn allow to constrain the Fe/Ni ratio in the core.

16 Here, we investigated the effect of nickel concentration in the metallic alloy on the partitioning

17 of other elements at conditions directly relevant to core formation, using the laser-heated

18 diamond anvil cell. We found no measurable effect of nickel concentration on the partitioning of

19 Ni, Cr and V; the Fe-Ni alloy is chemically ideal over a broad range of Ni concentrations (3.5 to

20 48.7 wt%). The ideality of the Fe-Ni solution across a wide range of nickel concentration shows

21 that Fe and Ni are not only twins from the standpoint for material properties, but also from that

22 of chemical properties in those high P-T conditions.

23 **Keywords:** Fe-Ni "ideality", core formation, metal-silicate partitioning, high pressure

INTRODUCTION

24

25   Earth's core is composed of Fe-Ni alloy with ~5-10 % of light element(s) to account for

26   the observed density deficit (Birch 1964). Assuming a chondritic bulk Earth and a known Fe/Ni

27   ratio in the bulk silicate Earth (BSE), the Fe/Ni ratio can be estimated using mass balance to be

28   ~16 in the core (Allègre et al. 1995; Mcdonough and Sun 1995). At outer-core conditions, the

29   effect of nickel content is negligible with respect to density, compressibility and wave velocities

30   (e.g., Lin et al., 2003; Kantor et al., 2007; Martorell et al., 2013; Badro et al. 2014). Therefore, it

31   is common practice to ignore Ni when simulating or experimenting on core properties. A recent

32   metal-silicate isotopic fractionation study (Elardo and Shahar 2017) found that nickel favors the

33   fractionation of heavy iron isotopes in the core during planetary core formation. This raises the

34   question whether nickel also affects the partitioning behavior of siderophile elements during core

35   formation, which in turn would affect our current understanding of core formation.

36   Core formation on Earth occurs by metal-silicate differentiation in a magma ocean (e.g.,

37   Ringwood 1959; Li and Agee 1996; Wood et al. 2006). Accreting material melts in the magma

38   ocean, and liquid metal separates and equilibrates with surrounding silicate melt as it

39   gravitationally segregates towards the center of the planet to form the core. This equilibration

40   process strips siderophile elements from the magma ocean (i.e., BSE) to the core, setting the

41   trace-element composition of both reservoirs. Their relative depletion in the BSE is obtained by

42   comparing the composition of the most primitive mantle-derived rocks with that of chondrites

43   (proxy for bulk Earth composition). High pressure and high temperature experiments can then be

44   used to match the observed depletions, and because metal-silicate partitioning is a function of

45   pressure (P), temperature (T), composition (X) and oxygen fugacity (fO$_2$), further constrain the

46   thermochemical conditions of core formation (e.g., Li and Agee 1996; Wade and Wood 2005;

47   Siebert et al. 2013; Fischer et al. 2015). Core formation models show that the P–T conditions for

48   metal-silicate equilibration range up to 75 GPa, with temperatures as high as 4350 K (Badro et

49   al. 2014), establishing that the core formed in a deep magma ocean. The presence of various

50   (major and trace) elements in liquid iron alloy have an influence on the partitioning of

51   siderophile trace elements, and extensive experiments have been designed to investigate the

52   effect of silicon, oxygen, carbon or sulfur (dissolved in metal) on element partitioning during

53   core formation; however, the effect of nickel, another major element in the core, has never been

54   experimentally tested, and it was always assumed that Ni-free or Ni-bearing systems behave

55   similarly from the point of view of partitioning.

EXPERIMENTS AND ANALYSIS

57   In this study, we investigated the effect of nickel on the metal-silicate partitioning of

58   three siderophile elements (Ni, Cr, V) by performing laser-heated diamond anvil cell (LHDAC)

59   experiments up to 94 GPa and 4500 K. Starting materials were synthesized at IPGP using a gas-

60   mixing aerodynamic levitation laser furnace (silicate) and a piston-cylinder press (metal). The

61   samples were polished and cut using a picosecond laser-machining system (IPGP) then loaded in

62   diamond anvil cells using rhenium gaskets and compressed to target pressures prior to heating

63   with a double-sided laser heating system (IPGP) to temperatures above the metal and silicate

64   liquidus, ensuring the samples were fully molten in each run. After quench and decompression, a

65   focused ion beam (FIB) instrument (Zeiss Auriga 40, IPGP) was used to extract thin sections

66   from the center of the laser-heated area (Fig. 1), which were analyzed on the same instrument

67   using quantitative energy dispersive X-ray (EDX) spectroscopy. Detailed description of the

68   experimental and analytical methods can be found in Supplemental Information. The

69   composition of the starting material can be found in Table S1.

4

RESULTS

70

71   Four diamond anvil cell experiments were performed at various P-T conditions and

72   summarized in Table S2, with metal phases displaying a range of Ni concentrations from 3.5 to

73   48.7 wt%.

74   The typical quench morphology consists of a spherical metallic blob (a few micrometers

75   in diameter) embedded in a silicate melt surrounded by untransformed glass (Fig. 1). Quench

76   texture in both silicate and metal was found in all experiments, similar to those seen in previous

77   superliquidus (i.e., molten silicate–molten metal) partition experiments in the LHDAC (Siebert et

78   al. 2012; Fischer et al. 2015; Badro et al. 2016; Blanchard et al. 2017). During quench, Si-O-rich

79   phases and Fe-Ni-rich blobs (< 200 nm) exsolved in the metal and silicate, respectively. Large

80   window (raster-scanned electron beam) was used whenever possible to average over quench

81   textures. Areas containing larger metallic blobs (0.5-2 μm in diameter) trapped in the silicate

82   were avoided during chemical analysis. The composition of quenched silicate and metal melts

83   from each run are reported in Table S3.

84   The partitioning of Ni, Cr and V between metal and silicate is the results of an exchange

85   reaction taking place between molten metal and silicate:

$$MO_{\frac{n}{2}} + \frac{n}{2}Fe = \frac{n}{2}FeO + M \#(1)$$
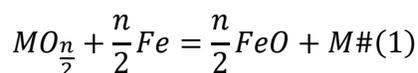
86   with a partition coefficient $D_M = x_M / x_{MOn/2}$, where n is the valence of the cation M in the silicate

87   and x the molar fraction of M. Partition coefficient is a function of P, T, composition and oxygen

88   fugacity. The exchange coefficient, $K_D(M) = D_M / D_{Fe}^{n/2}$, is the ratio of the partition coefficient

89   of element M to that of iron, and is therefore independent of iron concentrations in the metal and

5

90   silicate, i.e., the oxygen fugacity of the system. The equilibrium constant K of reaction (1) can be

91   defined in terms of the exchange coefficient and activity coefficients (γ) in the silicate and

92   metallic phases, and is related to the fundamental thermodynamic functions according to:

93
$$logK(M) = logK_D(M) + log\frac{\gamma_M^{metal}}{(\gamma_{Fe}^{metal})^{\frac{n}{2}}} + log\frac{(\gamma_{FeO}^{silicate})^{\frac{n}{2}}}{\gamma_{MO_{\frac{n}{2}}}^{silicate}} = a + \frac{b}{T} + \frac{c \cdot P}{T} \#(2)$$

94   where *a* is the entropy, *b* the enthalpy, and *c* the volume change of reaction (1). The ratio of

95   activity coefficients in silicate melt (3rd term in Eq. 2) is independent of melt composition in this

96   relatively narrow range of composition (O'Neill and Eggins 2002; Wade and Wood 2005;

97   O'Neill and Berry 2006) and it can safely be ignored; its thermal dependence (~1/T) is readily

98   integrated in the *a* and *b* constants of Eq. 2. However, the ratio of activity coefficients in the

99   metal can vary drastically with metal composition (Jana and Walker 1997a, 1997b; Tuff et al.

100   2011; Wood et al. 2014). We modelled them using the interaction parameter approach in a real

101   solution, a formally correct thermodynamic model (see Supplemental Information) at all

102   concentrations which has become a standard practice (e.g., Wade and Wood 2005; Corgne et al.

103   2009; Ricolleau et al. 2011; Siebert et al. 2013; Fischer et al. 2015) to calculate the activity

104   coefficients of γ_{Fe} and γ_i as a function of activity coefficients at infinite dilution (γ_i^0) and

105   interaction parameters (ε_i^j) that express the influence of element *j* on element *i* in the liquid iron.

106   Following previous studies (Corgne et al. 2008; Mann et al. 2009; Siebert et al. 2011) of the

107   valence of siderophile elements in silicate melts, we fixed the valence (*n* in Eq. 1) of Ni and Cr

108   to divalent (2+) and V to trivalent (3+).

109   **DISCUSSION**

110   Partitioning data on Ni, Cr and V from previous studies (Hillgren et al. 1996; Jana and

111   Walker 1997; Gessmann and Rubie 1998; Bouhifd and Jephcoat 2003, 2011; Chabot and Agee

6

112   2003; Wade and Wood 2005; Kegler et al. 2008; Mann et al. 2009; Siebert et al. 2012, 2013,

113   2011; Fischer et al. 2015) were compiled and plotted in Fig. 2, along with our data. The statistics

114   cover a wide range of P-T conditions: e.g., 99 data for Ni from 0 GPa and 1754 K to 100 GPa

115   and 5700 K. All the data used for our thermodynamic model can be found in Table S4-S6. In

116   order to avoid the spurious effects due to solute compositions (not to introduce an unnecessary

117   variability to the consolidated dataset), we only used data with no carbon (only with very few

118   exceptions in the case of Ni, which is insensitive to carbon, to better constrain the temperature

119   effect) and (virtually) no sulfur (concentrations < 0.1 mol%) in the system. The equilibrium

120   constant K was calculated using the interaction parameter model (Table 1), and then fitted to the

121   thermodynamic model described in Eq. 2, using multivariate least-squares linear regression.

122   Fitted thermodynamic parameters are listed in Table 1, and correspond to the dashed line plotted

123   alongside the data in Fig. 2.

124   For nickel, the least-squares regression for 99 data points shows a remarkable fit to Eq. 2

125   with R^2=0.923, and log K is plotted in Fig. 2a as a function of reciprocal temperature (x-axis)

126   and pressure (symbol color). As observed by several studies (e.g., Li and Agee 1996; Kegler et

127   al. 2008; Bouhifd and Jephcoat 2011; Siebert et al. 2012; Fischer et al. 2015), Ni becomes less

128   siderophile with increasing temperature ($b > 0$) and pressure ($c < 0$):

$$logK(Ni) = -0.40(22) + \frac{4454(430)}{T} - 58(8)\frac{P}{T} \#(3)$$

129   We find no significant compositional dependence across the wide range of Ni content in the

130   metal investigate here, which can be seen more clearly in Fig. 2b, where the equilibrium constant

131   (plotted in Fig. 2a) is adjusted to zero pressure, i.e., plotting a rewritten form of Eq. 3:

7

$$logK(Ni) + 58(8)\frac{P}{T} = -0.40(22) + \frac{4454(430)}{T} \#(4)$$

132   With all pressure-dependence cancelled out, the color now corresponds to the Ni concentration in

133   the metal, and the data for all Ni concentrations fall on a single linear trend; the broad range of

134   Ni concentration (from 3.5 to 48.7 wt%) demonstrates that there is no dependence of partitioning

135   on the nickel content in the metal. The absence of any deviation and excellent agreement

136   between our data and previous results provide a strong argument for the "neutrality" (with regard

137   to partitioning during core formation) of Ni in core-forming Fe–Ni alloy, with no observable

138   effect on its own partitioning from trace amounts up to 49 % of Ni in the metal under these

139   extreme P-T conditions.

140   Following the same procedure, Eq. 2 was fitted to chromium and vanadium partitioning

141   data using a least-squares linear regression, yielding:

$$logK(Cr) = -0.20(7) - \frac{2625(184)}{T} \#(5)$$

$$logK(V) = -1.83(12) - \frac{3433(313)}{T} \#(6)$$

142   Partitioning of both chromium and vanadium shows a strong positive temperature dependence

143   (b=-2625(184) K and -3433(313) K for Cr and V, respectively), indicating they become more

144   siderophile with increasing temperature, and no measurable dependence on pressure (c=0

145   K/GPa) as previously observed (e.g., Wood et al. 2008; Mann et al. 2009; Siebert et al. 2013)

146   and these are plotted in Figs. 2c and 2d. Again, despite nickel contents varying between 3.5 wt%

147   and 48.7 wt% in metal, the equilibrium constants obtained in our DAC experiments (Ni, Cr or V)

148   are intrinsically identical to those previously determined (within uncertainties), confirming

149 experimentally that nickel has also no measurable effect on the partitioning of Cr and V between

150 metal and silicate at the high P-T conditions of Earth's core formation.

151   It is also important to consider the effect of other light elements (e.g., sulfur and carbon)

152 because their strong influences on partitioning behavior. Carbon-unsaturated data were used in

153 this study (i.e., (Fischer et al. 2015) containing 3 to 16 mol% carbon in the metal) and show

154 excellent agreement with the C-free data in Figs. 2a and 2b. S-bearing data wasn't available at

155 high pressure and there is no indication whether S addition to the metal would change the

156 conclusion as observed at room pressure in the Fe-S and Ni-S end-members (e.g., Chabot et al.

157 2007).

158   **IMPLICATIONS**

159   Extensive metal-silicate partitioning experiments have been conducted over various P-T-

160 X conditions to constrain core formation. However, in order to obtain measurable concentrations

161 in both phases, unrealistic high content of trace elements is often inevitable. Unlike sulfur,

162 carbon or silicon, whose effects on partitioning are well studied and thus known to be of

163 importance, the influence of Ni has always been assumed negligible in experiments designed to

164 use pure Fe as starting material. For the first time, our DAC experiments performed at core-

165 formation conditions confirm the chemical "neutrality" of nickel in an iron alloy under these

166 extreme P-T conditions, over a wide range of nickel concentration.

167   **ACKNOWLEDGMENTS**

171   Community's Seventh Framework Programme (FP7/2007-2013) / ERC grant agreement n°

172   207467. We acknowledge the financial support of the UnivEarthS Labex program at Sorbonne

173   Paris Cité (ANR-10-LABX-0023 and ANR-11-IDEX-0005-02). Parts of this work were

174   supported by IPGP multidisciplinary program PARI, and by Paris–IdF region SESAME Grant no.

175   12015908.

176   **REFERENCES CITED**

177   Allègre, C.J., Poirier, J.P., Humler, E., and Hofmann, A.W. (1995) The chemical composition of

178   the Earth. Earth and Planetary Science Letters, 134, 515–526.

179   Badro, J., Cote, A.S., and Brodholt, J.P. (2014) A seismologically consistent compositional

180   model of Earth's core. Proceedings of the National Academy of Sciences, 111, 7542–7545.

181   Badro, J., Siebert, J., and Nimmo, F. (2016) An early geodynamo driven by exsolution of mantle

182   components from Earth's core. Nature, 536(7616), 326-328.

183   Birch, F. (1964) Density and composition of mantle and core. Journal of Geophysical Research,

184   69, 4377–4388.

185   Blanchard, I., Siebert, J., Borensztajn, S., and Badro, J. (2017) The solubility of heat-producing

186   elements in Earth's core. Geochemical Perspectives Letters, 5, 1–5.

187   Bouhifd, M.A., and Jephcoat, A.P. (2003) The effect of pressure on partitioning of Ni and Co

188   between silicate and iron-rich metal liquids: A diamond-anvil cell study. Earth and

189   Planetary Science Letters, 209, 245–255.

190   Bouhifd, M.A., and Jephcoat, A.P. (2011) Convergence of Ni and Co metal – silicate partition

191   coef fi cients in the deep magma-ocean and coupled silicon – oxygen solubility in iron melts

192   at high pressures. Earth and Planetary Science Letters, 307, 341–348.

193   Chabot, N.L., and Agee, C.B. (2003) Core formation in the Earth and Moon: New experimental

194   constraints from V, Cr, and Mn. Geochimica et Cosmochimica Acta, 67, 2077–2091.

195   Chabot, N.L., Saslow, S.A., McDonough, W.F., and McCoy, T.J. (2007) The effect of Ni on

196   element partitioning during iron meteorite crystallization. Meteoritics and Planetary

197   Science, 42, 1735–1750.

198   Corgne, A., Keshav, S., Wood, B.J., McDonough, W.F., and Fei, Y. (2008) Metal-silicate

199   partitioning and constraints on core composition and oxygen fugacity during Earth

200   accretion. Geochimica et Cosmochimica Acta, 72, 574–589.

201   Corgne, A., Siebert, J., and Badro, J. (2009) Oxygen as a light element: A solution to single-

202   stage core formation. Earth and Planetary Science Letters, 288, 108–114.

203   Elardo, S.M., and Shahar, A. (2017) Non-chondritic iron isotope ratios in planetary mantles as a

204   result of core formation. Nature Geoscience, 10, 317–321.

205   Fischer, R.A., Nakajima, Y., Campbell, A.J., Frost, D.J., Harries, D., Langenhorst, F., Miyajima,

206   N., Pollok, K., and Rubie, D.C. (2015) High pressure metal-silicate partitioning of Ni, Co,

207   V, Cr, Si, and O. Geochimica et Cosmochimica Acta, 167, 177–194.

208   Gessmann, C.K., and Rubie, D.C. (1998) The effect of temperature on the partitioning of nickel,

209   cobalt, manganese, chromium, and vanadium at 9 GPa and constraints on formation of the

210   Earth's core. Geochimica et Cosmochimica Acta, 62, 867–882.

211   Hillgren, V.J., Drake, M.J., and Rubie, D.C. (1996) High pressure and high temperature metal-

212   silicate partitioning of siderophile elements: The importance of silicate liquid composition.

213   Geochimica et Cosmochimica Acta, 60, 2257–2263.

214   Jana, D., and Walker, D. (1997) The impact of carbon on element distribution during core

215   formation. Geochimica et Cosmochimica Acta, 61, 2759–2763.

216   Jana, D., and Walker, D. (1997) The influence of silicate melt composition on distribution of

217   siderophile elements among metal and silicate liquids. Earth and Planetary Science Letters,

218   150, 463–472.

219   Jana, D., and Walker, D. (1997) The influence of sulfur on partitioning of siderophile elements.

220   Geochimica et Cosmochimica Acta, 61, 5255–5277.

221   Japan Society for the Promotion of Science and the Nineteenth Committee on Steelmaking.

222   (1988) Steelmaking Data Sourcebook. Gordon and Breach Science Publishers, New York.

223   Kantor, A.P., Kantor, I.Y., Kurnosov, A. V., Kuznetsov, A.Y., Dubrovinskaia, N.A., Krisch, M.,

224   Bossak, A.A., Dmitriev, V.P., Urusov, V.S., and Dubrovinsky, L.S. (2007) Sound wave

225   velocities of fcc Fe-Ni alloy at high pressure and temperature by mean of inelastic X-ray

226   scattering. Physics of the Earth and Planetary Interiors, 164, 83–89.

227   Kegler, P., Holzheid, A., Frost, D.J., Rubie, D.C., Dohmen, R., and Palme, H. (2008) New Ni

228   and Co metal-silicate partitioning data and their relevance for an early terrestrial magma

229   ocean. Earth and Planetary Science Letters, 268, 28–40.

230   Li, J., and Agee, C.B. (1996) Geochemistry of mantle–core differentiation at high pressure.

231   Nature, 381, 686-689.

232   Lin, J.-F. (2003) Sound velocities of iron-nickel and iron-silicon alloys at high pressures.

233   Geophysical Research Letters, 30, 2112.

234   Mann, U., Frost, D.J., and Rubie, D.C. (2009) Evidence for high-pressure core-mantle

235   differentiation from the metal-silicate partitioning of lithophile and weakly-siderophile

236   elements. Geochimica et Cosmochimica Acta, 73, 7360–7386.

237   Martorell, B., Brodholt, J., Wood, I.G., and Vočadlo, L. (2013) The effect of nickel on the

238   properties of iron at the conditions of Earth's inner core: Ab initio calculations of seismic

239   wave velocities of Fe-Ni alloys. Earth and Planetary Science Letters, 365, 143–151.

240   Mcdonough, W.F., and Sun, S. (1995) The composition of the earth. Chemical Geology, 120,

241   223-253.

242   O'Neill, H.S.C., and Berry, A.J. (2006) Activity coefficients at low dilution of CrO, NiO and

243   CoO in melts in the system CaO-MgO-Al2O3-SiO2at 1400°C: Using the thermodynamic

244   behaviour of transition metal oxides in silicate melts to probe their structure. Chemical

245   Geology, 231, 77–89.

246   O'Neill, H.S.C., and Eggins, S.M. (2002) The effect of melt composition on trace element

247   partitioning: An experimental investigation of the activity coefficients of FeO, NiO, CoO,

248   MoO2 and MoO3 in silicate melts. Chemical Geology, 186, 151–181.

249   Ricolleau, A., Fei, Y., Corgne, A., Siebert, J., and Badro, J. (2011) Oxygen and silicon contents

250   of Earth's core from high pressure metal-silicate partitioning experiments. Earth and

251   Planetary Science Letters, 310, 409–421.

252   Ringwood, A.E. (1959) On the chemical evolution and densities of the planets. Geochemica et

253   Cosmochimica Acta, 15, 257–283.

254   Siebert, J., Corgne, A., and Ryerson, F.J. (2011) Systematics of metal-silicate partitioning for

255   many siderophile elements applied to Earth's core formation. Geochimica et Cosmochimica

256   Acta, 75, 1451–1489.

257   Siebert, J., Badro, J., Antonangeli, D., and Ryerson, F.J. (2012) Metal-silicate partitioning of Ni

258   and Co in a deep magma ocean. Earth and Planetary Science Letters, 321–322, 189–197.

259   Siebert, J., Badro, J., Antonangeli, D., and Ryerson, F.J. (2013) Terrestrial Accretion Under

260   Oxidizing Conditions. Science, 339, 1194-1197.

261   Tuff, J., Wood, B.J., and Wade, J. (2011) The effect of Si on metal-silicate partitioning of

262   siderophile elements and implications for the conditions of core formation. Geochimica et

263   Cosmochimica Acta, 75, 673–690.

264   Wade, J., and Wood, B.J. (2005) Core formation and the oxidation state of the Earth. Earth and

265   Planetary Science Letters, 236, 78–95.

266   Wood, B.J., Walter, M.J., and Wade, J. (2006) Accretion of the Earth and segregation of its core.

267   Nature, 441, 825–833.

268   Wood, B.J., Wade, J., and Kilburn, M.R. (2008) Core formation and the oxidation state of the

269   Earth: Additional constraints from Nb, V and Cr partitioning. Geochimica et Cosmochimica

270   Acta, 72, 1415–1426.

271   Wood, B.J., Kiseeva, E.S., and Mirolo, F.J. (2014) Accretion and core formation: The effects of

272   sulfur on metal-silicate partition coefficients. Geochimica et Cosmochimica Acta, 145, 248–

273   267.

274

275

276   **Figure captions:**

277   **FIGURE 1.** Backscattered electron image of a FIB section recovered from a super-liquidus

278   metal-silicate equilibration at 73 GPa and 4300 K in the laser-heated diamond anvil cell.

279   **FIGURE 2.** Equilibrium constants (log K) for Ni, Cr and V as a function of reciprocal

280   temperature (1000/T). The dashed lines correspond to least-squares linear regressions to the data,

281   and error bars (only for the data from this study, shown where larger than symbols) were

282   propagated from the analytical uncertainties in Table S3. **(a)** Ni. Experimental data are taken

283   from (Hillgren et al. 1996; Jana and Walker 1997; Gessmann and Rubie 1998; Bouhifd and

284   Jephcoat 2003, 2011; Kegler et al. 2008; Siebert et al. 2011, 2012, 2013; Fischer et al. 2015) and

285   this study (squares). Pressure is reported in symbol color. **(b)** Equilibrium constant for Ni

286   adjusted to 0 pressure (i.e., log K $-$ c P/T) as a function of reciprocal temperature, for the same

287   data as in (a). Symbol color corresponds to Ni concentration (molar fraction) in liquid metal. **(c–**

288   **d)** Cr and V equilibrium constant (log K) versus reciprocal temperature. Experimental data are

289   taken from (Hillgren et al. 1996; Jana and Walker 1997; Gessmann and Rubie 1998; Bouhifd and

290   Jephcoat 2003, 2011; Chabot and Agee 2003; Wade and Wood 2005; Kegler et al. 2008; Mann et

291   al. 2009; Siebert et al. 2012, 2013, 2011; Fischer et al. 2015) and this study (squares).

292

293   **TABLE 1.** Thermodynamic parameters of the metal-silicate partitioning of Ni, Cr and V.

Element (i)	a	b (K)	c (K/GPa)	ε_i^O	ε_i^{Si}	ε_i^i	$\ln\gamma_i^0$	N	R^2
Ni	-0.40(22)	4454(430)	-58(8)	**-6.2**	1.16	0	-0.42	99	0.923
Cr	-0.20(7)	-2625(184)	0	**-8.8**	0	0	0	45	0.825
V	-1.83(12)	-3433(313)	0	**-24.4**	**4.4**	6.57	-2.53	46	0.732
O					-5	-1			
Si						12.4			

294   Notes: Parameters of Eq. 2 for Ni, Cr and V partitioning: a, b and c represent the entropy,
295   enthalpy and volume change of the reaction, values in parenthesis are standard errors (1 σ)
296   obtained from the least-squares regressions. ε_i^j is the interaction parameter of element j on
297   element i and γ_i^0 the activity coefficient of solute i at infinite dilution in liquid iron; interaction

15

298   parameters in boldface are calculated from this study, other values are taken from *Steelmaking*
299   *Data Sourcebook* (1988). Interaction parameters and activity coefficients are reported at 1873 K
300   (details are given in Supplementary Information). N is the number of data used in each
301   thermodynamic modeling, and R^2 the coefficient of determination of the fitted model.

2 μm